MATERIALS RESEARCH LETTERS

*Mater. Res. Lett.*, 2015
Vol. 3, No. 1, 30–34, http://dx.doi.org/10.1080/21663831.2014.958586

Taylor & Francis
Taylor & Francis Group

www.tandfonline.com/toc/tmrl20/current

# Effect of Microstructure on the Deformation Mechanism of Friction Stir-Processed $Al_{0.1}CoCrFeNi$ High Entropy Alloy

M. Komarasamy[a], N. Kumar[a], Z. Tang[b], R.S. Mishra[a*], and P.K. Liaw[b]

[a]*Department of Materials Science and Engineering, Center for Friction Stir Processing, University of North Texas, Denton, TX 76203, USA;* [b]*Department of Materials Science and Engineering, The University of Tennessee, Knoxville, TN 37996, USA*

(*Received 7 August 2014; final form 22 August 2014*)

Grain refinement from several millimeters in as-received (AR) condition to the range of 0.35–15 μm was achieved by friction stir processing (FSP). Due to the sluggish nature of atomic diffusion in high entropy alloys (HEAs), the FSP region exhibited an immense variation in microstructure which was directly attributed to the accumulated plastic strain during FSP. In accordance with the Hall–Petch relationship, yield strength (YS) has increased by a factor of four after grain refinement while maintaining large uniform elongation (UE). The Kocks–Mecking plot indicated different deformation mechanisms operative in both FSP and AR conditions.

**Keywords:** Grain Refinement, Strain Gradient, Work Hardening, Twinning

High entropy alloys (HEAs) are new class of materials, which consist of equimolar or near-equimolar compositions of minimum five principal alloying elements. They tend to form random solid solutions with simple crystal structures [face-centered-cubic (FCC) and/or body-centered-cubic (BCC)], synthesized based on Boltzmann's hypothesis of maximizing the configurational entropy by increasing the number of elements added in the alloy system.[1–8]

So far, microstructure and mechanical properties have been evaluated for various HEA systems, but in-depth analysis on the deformation mechanism of HEA is still lacking.[9–12] Recently, Otto et al. [13] studied the underlying deformation mechanisms in CoCrFeMnNi HEA in both fine-grained (FG) and coarse-grained (CG) materials, and elucidated the role of twinning when deformed at 77 K. So far, cold rolling and subsequent annealing treatments have been carried out to obtain grain refinement in HEAs.[13–15] Due to severe lattice distortion and sluggish diffusion, HEAs exhibit rather a high recrystallization temperature ($\sim 0.62T_m$).[14] Moreover, grain coarsening in CoCrFeMnNi HEA was observed only when the recrystallized sample was annealed at 850°C.[15] Generally, these factors will play a crucial role in the microstructural evolution during any thermo-mechanical processing.

Friction stir processing (FSP) [16] has proven to be an effective tool for microstructural modification of Al,[17] Mg,[18] Ti [19] alloys and steels.[20] So far, no one has attempted to refine the grain size in HEA using an FSP technique. The Hall–Petch relationship predicts a dependence of yield strength (YS) on grain size. Hence, FSP-assisted grain refinement is expected to increase the YS of the alloy. Moreover, there is a lack of understanding about the work-hardening or deformation mechanism as a function of grain size (both CG and FG regimes) in HEAs. In this letter, we are reporting (i) grain refinement using FSP and a detailed study on the microstructural evolution at various locations in the processed region using scanning electron microscopy (SEM). In addition, (ii) the effect of grain refinement on the tensile properties and the underlying deformation mechanisms in both CG and FG materials have been addressed.

A vacuum-induction melted and hot-isostatically pressed ~4.0 mm thick $Al_{0.1}CoCrFeNi$ HEA was subjected to FSP. A cylindrical tungsten carbide tool with 1.5 mm pin height was used to process the material. The

*Corresponding author. Email: rajiv.mishra@unt.edu

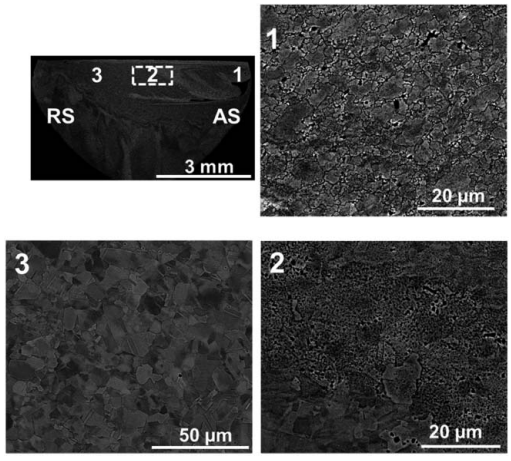


Figure 1. SEM micrographs taken at various locations in the friction stir-processed region. The locations are marked along with the location of cross-section of the mini-tensile sample gage on the macro view of the processed region.

following FSP process parameters were used: a tool rotation rate of 1000 revolutions per minute, tool traverse speed of 25.4 mm per minute, tool tilt angle of 0.5° and a plunge depth of 1.80 mm. The cross-section of the processed region was polished and analyzed using SEM. Mini-tensile testing was carried out in both CG and FG conditions at an initial strain rate of $1 \times 10^{-3}$ $s^{-1}$ at room temperature. The mini-tensile sample location in FG condition is shown as a dotted white rectangle on the macro cross-section of the processed region, in Figure 1. The dotted rectangular region represents the gage cross-section of the mini-tensile sample, with the width and thickness being 1.25 and 0.6 mm, respectively. The gage length of the tested sample was 2 mm and it was oriented along the processed direction. Transmission electron microscopy (TEM) samples were extracted from the fractured tensile sample in the CG condition and prepared using a regular procedure. The final thinning was done using a precision ion polishing system. TEM analysis of the failed sample was carried out in Technai G2 F20 STEM. The surface reliefs on the failed sample in FG condition were analyzed using SEM. X-ray diffraction (XRD) was used for phase characterization.

Based on both the XRD and SEM analysis, the studied HEA is a single phase alloy with an FCC crystal structure. In as-received (AR) condition, the grains were on the order of few millimeter in size. In this microstructural condition, the alloy was subjected to FSP to refine the grain size. Figure 1 shows the SEM micrographs taken at various locations in the processing region. The micrographs are marked with numbers, and the corresponding locations are shown in the macro view of the processed region. Micrographs 1, 2 and 3 were taken at the advancing side (AS), the center and the retreating side (RS) of the processing region, respectively. The presence of filling defect at the AS can be seen in the macro view of the nugget. Grain size in the AS was in the range of 0.35–3 μm and in the RS, it was in the range of 2–13.5 μm. Several annealing twins were also observed in the RS, which were absent in the AS. Although the microstructural evolution was inhomogeneous in the processed region; overall, a significant grain refinement was achieved in HEA by FSP in a single step.

Figure 2(a) shows the hardness variation across the processed region. The hardness variation can be directly correlated to the variation in grain size in the processed region. There were three levels of hardness observed and marked as regions 1, 2 and 3. Region 1 exhibited higher hardness due to finer grains in the AS, followed by region 2, a transition region, which was due to the non-recrystallized zones observed in between recrystallized regions and then by region 3, which possessed lower hardness due to the presence of relatively coarse grains. The observed hardness variation in the processed region is unique to the HEA and was not observed in the friction stir-processed region of any other alloy systems.[21–23]

Hence, a better understanding of the microstructural evolution at various regions becomes necessary, since it directly impacts the mechanical properties. Generally, microstructural evolution, dynamic recrystallization and

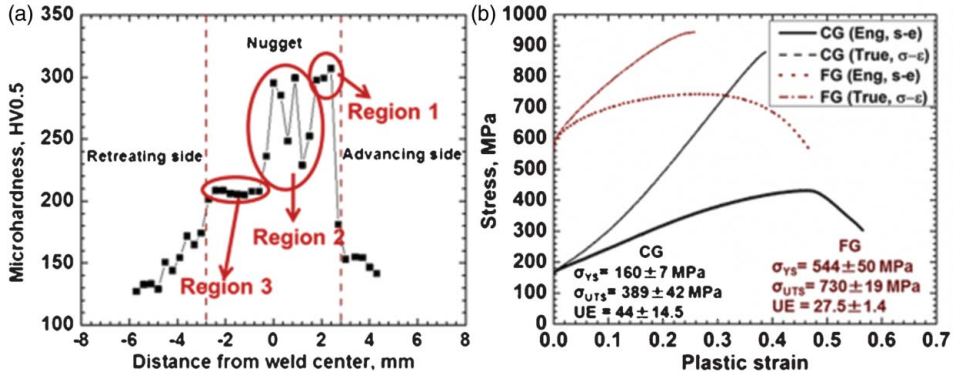


Figure 2. (a) The variation of hardness across the processed region on the transverse cross section and (b) the plastic stress–strain curves in both CG and FG conditions.

grain growth during FSP is controlled by strain, strain rate and temperature experienced by that local region. It is widely known that the dynamic recrystallization during thermo-mechanical processing of low stacking fault energy (SFE) materials is mainly via discontinuous dynamic recrystallization (DDRX).[24] Zaddach et al. [25] calculated the SFE of NiFeCoCr HEA using DFT calculations and XRD analysis, and found it to be as low as 17 $mJ/m^2$. Therefore, it is highly likely that DDRX was a dominant recrystallization mechanism during FSP of HEA. Moreover, the low SFE limits the role of dynamic recovery during thermo-mechanical processing, hence results in a higher fraction of stored dislocations. These dislocation structures and grain boundaries act as nucleation sites for the recrystallized nuclei during both dynamic and static recrystallization. In a given region, the number density of the nucleation sites will increase with the accumulated plastic strain. In FSP, AS experiences larger plastic strain as compared with the RS [20]; hence, results in a higher and lower fraction of recrystallized nuclei in the AS and RS, respectively.

Upon the completion of dynamic recrystallization, grain growth might occur during the cooling cycle, depending on both the thermodynamic and kinetic factors; such as temperature, time, total grain boundary energy and diffusivity of the atoms. In single phase materials with high self-diffusivity, significant grain growth after dynamic recrystallization is unavoidable in the processed region during the cooling cycle. On the contrary, sluggish diffusion of atoms in HEA systems will likely to have a major impact on the grain growth during the cooling cycle of the friction stir process. Therefore, in the absence of second-phase particles to pin the grain boundaries (the present alloy is a single-phase FCC material), it is the sluggish diffusion that controlled and retarded the grain growth during the cooling cycle, which is unique to materials like HEAs. Hence, the observed variation in grain size in the processed region is justified, where AS displayed very fine grain size and RS displayed comparatively coarser grains. Given the small size of the processed region, the differences in the thermal cycles of AS and RS locations are likely to be insignificant. As shown, such variations in microstructure locally also result in local variation in mechanical properties [Figure 2(a)].

Figure 2(b) shows the engineering and true stress–strain curves in both CG and FG conditions. YS, ultimate tensile strength (UTS) and uniform elongation (UE) values in both CG and FG conditions are shown in Figure 2(b). Since the FS processed region possessed inhomogeneous microstructure, great care was taken to extract a representative gage section which contains both ultrafine and fine grains. First point to be noted here is the effect of the grain size on YS, which was nearly fourfold higher after the grain refinement. Secondly, the extensive work-hardening ability observed in both CG and FG HEA materials. Thirdly, the difference in the shape of the stress–strain curves in both FG and CG conditions, which indicates the on-going deformation mechanisms. Detailed reasoning for the observed deformation mechanism will be discussed in the forthcoming section.

Work-hardening curves in both CG and FG conditions are shown in Figure 3. Though, there has been discussions on HEA possessing higher work-hardening ability, so far, no one has reported on the work-hardening behavior, $d\sigma/d\varepsilon$, and discussed the deformation mechanisms operating at various stages of the work-hardening curve. A simple hardening curve (a polynomial fit to the true stress–strain curve) was chosen rather than power-law-hardening curve (power law fit to the true stress–strain curve) to exaggerate the inflection point and the variation in slope. The effect of grain size on the work-hardening behavior can be clearly seen. In the CG material, three distinct stages of work hardening were observed, marked as stages A, B and C. The decrease in the work-hardening rate in stage A signifies the dislocation-controlled plasticity, and it resembles stage III of high SFE material, a recovery-dominated regime. In Figure 3, point ‘a’ marks the transition from stage A to B. Detailed TEM analysis has been carried out in the past to correlate this transition to the onset of twinning deformation.[26] Stage B is characterized by an increase in the work-hardening rate due to the introduction of twins in the microstructure. The presence of twins in the microstructure presents an effective barrier to dislocation motion and reduces the mean free path of the dislocation. In addition, the dislocations will interact with twin boundaries resulting in increased dislocation storage inside the grains at the twin–matrix interface. This appears to be the main reason for the exceptional work hardening observed in stage B of the CG material. By comparing the work-hardening curve of HEA in the CG condition with other low SFE materials, such as Cu alloys and TWIP steels,[27] the increase in work-hardening rate during stage B is very high and is unique to HEA. Point ‘b’ marks the transition from stage B to C, which is again a slip-dominated regime and can be seen from the decreasing work-hardening rate.

The effect of grain size on twinning has received due attention in the past in low SFE materials. It has been proved that with a reduction in grain size, twin nucleation is suppressed in TWIP steels and Cu alloys.[27] Though, the work-hardening behavior of the FG material is different from the CG material, it still exhibited three stages of hardening. The FG material exhibited the same work-hardening behavior as the CG material only in stage C. The slope, rate of recovery, in stage A is shallower in the FG material as compared with the CG material. The interesting part in the work-hardening

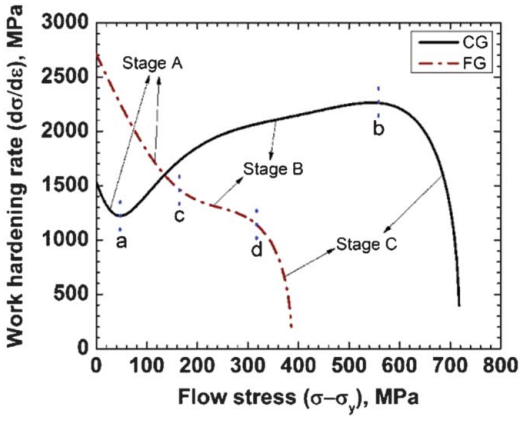


Figure 3. The variation of the work-hardening rate against the flow stress in both CG and FG conditions is shown. Note the difference in stage B of the two curves.

curve of FG material as compared with the CG material behavior is stage B. The work-hardening rate in stage B was continuously decreasing with stress, but at a slower rate as compared with the rate drop related to any recovery-related phenomena. From the literature observations of stage B in various low SFE alloys,[27] the work-hardening behavior observed in stage B of the FG material does indeed have contribution from twinning. The observed stage B behavior in the FG can be explained in two possible ways. First, the reduction in the twin density in the FG material reduced the barrier to dislocation motion. Second possibility is based on the interaction between the twins and dislocations. If the twin orientation was parallel rather than at 70.5° to the primary slip system, and if there was very limited activation of the secondary slip system, then the interaction between the dislocations and twins will be reduced. This will greatly impact the work-hardening rate in the twin-dominated regime.

It is well established that both yield stress ($\sigma_y$) and twinning stress ($\sigma_T$) greatly depend on the grain size and follows the Hall–Petch type relationship [28]:

$$\sigma_y \text{ or } \sigma_T = \sigma_0 + K_{S \text{ or } T} d^{-1/2}, \quad (1)$$

where $\sigma_0$ is the friction stress, $d$ is the grain size, and $K_s$ and $K_T$ are the Hall–Petch constants for slip and twinning, respectively. This model is based on the critical pile-up stress required at the grain boundary to nucleate a twin or to cause slip in the neighboring grain. For a given material, the stress to nucleate twins increases with the reduction in grain size. Based on the stress–strain curve, the twinning stress, initiation of stage B, in the FG material was 140 MPa (point c in Figure 3) and is quite large, as compared with the twinning stress in the CG material, which was 43 MPa (point a in Figure 3). The effect of grain size on the change in the deformation mechanism of the HEA can be clearly seen from this study.

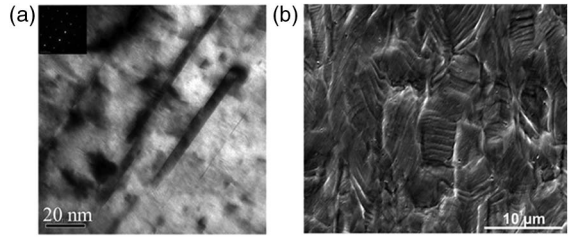


Figure 4. (a) TEM multi-beam bight field image of a deformed specimen showing the presence of twins in the CG material. (b) SEM surface micrograph showing the slip traces in the FG material after deformation to failure.

Figure 4(a) shows a TEM micrograph of the post deformation analysis carried out in the failed CG tensile sample. The presence of nanoscale deformation twins can be seen from the TEM micrograph, and the corresponding selected area diffraction pattern is shown in the inset. There were no micron-sized twins present in the deformed tensile sample, and only one set of twin orientation was observed. The observation of nano-sized deformation twins explains the exceptional work-hardening rate observed in stage B, and its uniqueness as compared with other low SFE materials, which had micron-sized twins. Figure 4(b) shows the SEM micrograph of surface slip markings observed in the FG material after tensile deformation. From the analysis of the slip traces in various grains, there was no observation of slip lines oriented in multiple directions or intersecting with each other, which implies that only the primary slip system was active in most of the grains. This will greatly reduce the twin–dislocation interactions, which could probably be the reason for the reduced work-hardening rate in stage B of the FG material.

In summary, extensive grain size reduction was obtained by FSP. The processed region exhibited a unique variation in the grain size, as compared with other metallic alloys. Variation in microstructural evolution across the processing region was attributed to the difference in the strain accumulation and sluggish nature of diffusion. Extensive work-hardening ability in the CG material was due to the presence of nanoscale deformation twins. A significant increase in YS was observed after grain refinement. The change in the work-hardening mechanism with the reduction in grain size was explained in terms of the limited dislocation–twin interactions.

**Acknowledgement** We would like to thank Center for Advanced Research and Technology (CART) for the microscopy facilities.

## References

[1] Yeh JW, Chen SK, Lin SJ, Gan JY, Chin TS, Shun TT, Tsau CH, Chang SY. Nanostructured high-entropy alloys

with multiple principal elements: novel alloy design concepts and outcomes. Adv Eng Mater. 2004;6:299–303.
[2] Hemphill MA, Yuan T, Wang GY, Yeh JW, Tsai CW, Chuang A, Liaw PK. Fatigue behavior of $Al_{0.5}$CoCrCuFeNi high entropy alloys. Acta Mater. 2012;60:5723–5734.
[3] Senkov ON, Wilks GB, Miracle DB, Chuang CP, Liaw PK. Refractory high-entropy alloys. Intermetallics. 2010;18:1758–1765.
[4] Tang Z, Gao MC, Diao H, Yang T, Liu J, Zuo T, Zhang Y, Lu Z, Cheng Y, Zhang Y, Dhamen KA, Liaw PK, Egami T. Aluminum alloying effects on lattice types, microstructures, and mechanical behavior of high-entropy alloys systems. J Mater Sci. 2013;65:1848–1858.
[5] Tang Z, Huang L, He W, Liaw PK. Alloying and processing effects on the aqueous corrosion behavior of high-entropy alloys. Entropy. 2014;16:895–911.
[6] Zhang Y, Zhou YJ, Lin JP, Chan GL, Liaw PK. Solid-solution phase formation rules for multi-component alloys. Adv Eng Mater. 2008;10:534–538.
[7] Zhang Y, Zuo T, Cheng Y, Liaw PK. High-entropy alloys with high saturation magnetization, electrical resistivity, and malleability. Sci Rep. 2013;3:1455–1461.
[8] Zhang Y, Zuo TT, Tang Z, Gao MC, Dahmen KA, Liaw PK, Lu ZP. Microstructures and properties of high-entropy alloys. Prog Mater Sci. 2014;61:1–93.
[9] Zhang KB, Fu ZY, Zhang JY, Wang WM, Wang H, Wang YC, Zhang QJ, Shi J. Microstructure and mechanical properties of CoCrFeNiTi$Al_x$ high-entropy alloys. Mater Sci Eng A. 2009;508:214–219.
[10] Gali A, George EP. Tensile properties of high- and medium-entropy alloys. Intermetallics. 2013;39:74–78.
[11] Shun TT, Du YC. Microstructure and tensile behaviors of FCC $Al_{0.3}$CoCrFeNi high entropy alloy. J Alloys Compd. 2009;479:157–160.
[12] Wang YP, Li BS, Ren MX, Yang C, Fu HZ. Microstructure and compressive properties of AlCrFeCoNi high entropy alloy. Mater Sci Eng A. 2008;491:154–158.
[13] Otto F, Dlouhý A, Somsen Ch, Bei H, Eggeler G, George EP. The influences of temperature and microstructure on the tensile properties of a CoCrFeMnNi high-entropy alloy. Acta Mater. 2013;61:5743–5755.
[14] Bhattacharjee PP, Sathiaraj GD, Zaid M, Gatti JR, Lee C, Tsai CW, Yeh JW. Microstructure and texture evolution during annealing of equiatomic CoCrFeMnNi high-entropy alloy. J Alloys Compd. 2014;587:544–552.
[15] Liu WH, Wu Y, He JY, Nieh TG, Lu ZP. Grain growth and the Hall–Petch relationship in a high-entropy FeCrNiCoMn alloy. Scripta Mater. 2013;68:526–529.
[16] Mishra RS, Mahoney MW, McFadden SX, Mara NA, Mukherjee AK. High strain rate superplasticity in a friction stir processed 7075 Al alloy. Scripta Mater. 1999;42:163–168.
[17] Kumar N, Mishra RS, Huskamp CS, Sankaran KK. Microstructure and mechanical behavior of friction stir processed ultrafine grained Al–Mg–Sc alloy. Mater Sci Eng A. 2011;528:5883–5887.
[18] Chang CI, Du XH, Huang JC. Achieving ultrafine grain size in Mg–Al–Zn alloy by friction stir processing. Scripta Mater. 2007;57:209–212.
[19] Su J, Wang J, Mishra RS, Xu R, Baumann JA. Microstructure and mechanical properties of a friction stir processed Ti–6Al–4V alloy. Mater Sci Eng A. 2013;573:67–74.
[20] Sato YS, Nelson TW, Sterling CJ, Steel RJ, Pettersson CO. Microstructure and mechanical properties of friction stir welded SAF 2507 super duplex stainless steel. Mater Sci Eng A. 2005;397:376–384.
[21] Zhang Y, Sato YS, Kokawa H, Park SHC, Hirano S. Microstructural characteristics and mechanical properties of Ti–6Al–4V friction stir welds. Mater Sci Eng A. 2008;485:448–455.
[22] Reynolds AP, Tang W, Khandkar Z, Khan JA, Lindner K. Relationships between weld parameters, hardness distribution and temperature history in alloy 7050 friction stir welds. Sci Technol Weld Join. 2005;10:190–199.
[23] Saeid T, Abdollah-zadeh A, Assadi H, Ghaini FM. Effect of friction stir welding speed on the microstructure and mechanical properties of a duplex stainless steel. Mater Sci Eng A. 2008;496:262–268.
[24] Wang Y, Shao WZ, Zhen L, Zhang XM. Microstructure evolution during dynamic recrystallization of hot deformed superalloy 718. Mater Sci Eng A. 2008;486:321–332.
[25] Zaddach AJ, Niu C, Koch CC, Irving DL. Mechanical properties and stacking fault energies of NiFeCrCoMn high-entropy alloy. J Mater Sci. 2013;65:1780–1789.
[26] Asgari S, El-Danaf E, Kalidindi SR, Doherty RD. Strain hardening regimes and microstructural evolution during large strain compression of low stacking fault energy fcc alloys that form deformation twins. Metall Mater Trans A. 1997;28:1781–1795.
[27] El-Danaf E, Kalidindi SR, Doherty RD. Influence of grain size and stacking-fault energy on deformation twinning in fcc metals. Metall Mater Trans A. 1999;30:1223–1233.
[28] Meyers MA, Vöhringer O, Lubarda VA. The onset of twinning in metals: a constitutive description. Acta Mater. 2001;49:4025–4039.